




Article

A Selenophene-Incorporated Metal–Organic Framework for Enhanced CO₂ Uptake and Adsorption Selectivity

Pavel A. Demakov ^{1,2}, Sergey S. Volynkin ¹, Denis G. Samsonenko ^{1,2},
Vladimir P. Fedin ^{1,2,*} and Danil N. Dybtsev ^{1,2}

¹ Nikolaev Institute of Inorganic Chemistry, Siberian Branch of the Russian Academy of Sciences, Novosibirsk 630090, Russia; demakov@niic.nsc.ru (P.A.D.); volynkin@niic.nsc.ru (S.S.V.); denis@niic.nsc.ru (D.G.S.); dan@niic.nsc.ru (D.N.D.)

² Department of Natural Sciences, Novosibirsk State University, 2 Pirogova St., Novosibirsk 630090, Russia

* Correspondence: cluster@niic.nsc.ru

Received: 2 September 2020; Accepted: 22 September 2020; Published: 24 September 2020



Abstract: A new metal–organic coordination polymer [Zn₂(sedc)₂(dabco)] (**1se**; sedc^{2−} = selenophene-2,5-dicarboxylate; dabco = 1,4-diazabicyclo[2.2.2]octane) was synthesized and characterized by single-crystal X-ray diffraction analysis. This MOF is based on {Zn₂(OOCR)₄N₂} paddle wheels and is isorecticular to the family of [Zn₂(bdc)₂(dabco)] derivatives (**1b**; bdc^{2−} = 1,4-benzenedicarboxylate) with **pcu** topology. The gas adsorption measurements revealed that **1se** shows a 15% higher CO₂ volumetric uptake at 273 K and 28% higher CO₂ uptake at 298 K (both at 1 bar) compared to the prototypic framework **1b**. Methane and nitrogen adsorption at 273 K was also investigated, and IAST calculations demonstrated a pronounced increase in CO₂/CH₄ and CO₂/N₂ selectivity for **1se**, compared with **1b**. For example, the selectivity factor for the equimolar CO₂/CH₄ gas mixture at 1 bar = 15.1 for **1se** and 11.9 for **1b**. The obtained results show a remarkable effect of the presence of selenium atom on the carbon dioxide affinity in the isorecticular metal–organic frameworks with very similar geometry and porosity.

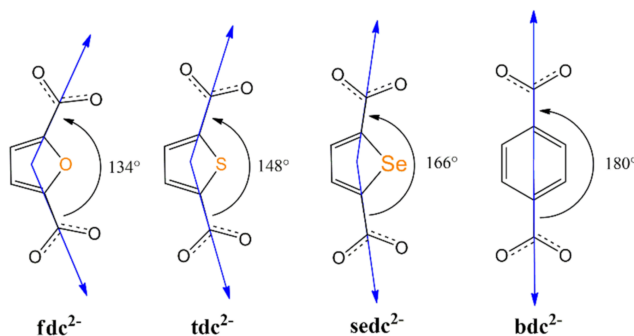
Keywords: porous metal–organic frameworks; selenophene; X-ray diffraction studies; adsorption measurements; gas adsorption selectivity

1. Introduction

Carbon dioxide is a corrosive gas and a major atmospheric pollutant, causing a greenhouse effect. Selective capture and sequestration of carbon dioxide is one of the challenging problems in the modern chemical industry. Typically, a chemical sorption of CO₂ by amines is highly effective; however, the corrosive nature of the chemisorbents and substantial energy penalties during their regeneration demand new viable alternatives [1–4]. Porous coordination polymers or metal–organic frameworks (MOFs) are recently emerged materials with the greatest potential for adsorption of gases. Remarkable porosity, sufficient stability, as well as vast versatility of the structural and functional design make this class of porous materials among the most perspective adsorbents for selective CO₂ capture from natural gas or industrial flue gas [5–10]. Modular design is a widely used principle to tailor structural and/or functional properties within a certain type of isostructural MOF family, such as IRMOF-1 [11–13], MIL-53 [14–16], or UiO-66 [17–19], which are typically based on the linear 1,4-benzenedicarboxylate (bdc^{2−}) linker. Other than a bent shape, the striking feature of ditopic dicarboxylate linkers based on heterocyclic core (Scheme 1) is the polarity of the core and the polarizability of a heteroatom, enabling additional induced dipole interactions with a substrate. Recently, a number of research groups have shown that the incorporation of 2,5-furandicarboxylate (fdc^{2−}) or

2,5-thiophenedicarboxylate (tdc^{2-}) into porous MOF structures imbue such materials with quite unique features such as selective ion adsorption, luminescence sensing [20–22], dielectric bistability [23], and gas/vapor uptake [24,25].

A porous coordination polymer $[\text{Zn}_2(\text{bdc})_2(\text{dabco})]$ (dabco = 1,4-diazabicyclo[2.2.2]octane) is a prototypic compound of a bountiful MOF family with highly tunable structural features [26–30]. We have demonstrated that the incorporation of 2,5-thiophenedicarboxylate instead of the 1,4-benzenedicarboxylate into this MOF enhances both the CO_2 adsorption uptake and the CO_2/N_2 adsorption selectivity of $[\text{Zn}_2(\text{tdc})_2(\text{dabco})]$ by as much as 50%, compared with the original structure $[\text{Zn}_2(\text{bdc})_2(\text{dabco})]$ at the same conditions [31]. The single-crystal X-ray diffraction studies, as well as the quantum-chemical calculations unveiled the role of the thiophene moieties in the specific CO_2 binding via an induced dipole interaction between CO_2 molecules and the heterocycle. Selenium atoms possess even greater radius and higher polarizability than sulfur. Thus, an enhancement of adsorption properties owing to van der Waals intermolecular interactions between a MOF and CO_2 or other gaseous substrate should be expected if a selenophene moiety is incorporated into such porous material. The 2,5-selenophenedicarboxylate (sedc^{2-}) is the heterocyclic linker, structurally and functionally similar to the 2,5-thiophenedicarboxylate. Except for a handful of examples [32,33], sedc^{2-} has mostly been ignored in MOF chemistry so far. Herein, we report the synthesis and investigation of a new selenophenedicarboxylate-based porous MOF $[\text{Zn}_2(\text{sedc})_2(\text{dabco})]$ (**1se**), which is isorecticular to both $[\text{Zn}_2(\text{bdc})_2(\text{dabco})]$ (**1b**) and $[\text{Zn}_2(\text{tdc})_2(\text{dabco})]$ (**1t**). The impact of selenium heteroatom on the adsorption properties of $[\text{Zn}_2(\text{sedc})_2(\text{dabco})]$ is discussed in detail.



Scheme 1. Structural formulae of fdc^{2-} , tdc^{2-} , sedc^{2-} , and bdc^{2-} dicarboxylate linkers.

2. Results and Discussion

2.1. Structure Description

The coordination polymer **1se** was synthesized by the solvothermal reaction of $\text{Zn}(\text{NO}_3)_2 \cdot 6\text{H}_2\text{O}$, H_2sedc , and dabco in DMF at $100\text{ }^\circ\text{C}$ for 24 h. According to single-crystal X-ray diffraction data, **1se** crystallizes in the tetragonal space group $P-42_1c$. The asymmetric unit contains two crystallographically independent Zn(II) atoms with the same coordination environment of four O atoms of four bridging carboxylate groups and one N atom of dabco bridge. Zn–O distances lie in the range 2.015(2)–2.062(2) Å. Zn–N distances are 2.040(2) and 2.047(2) Å. Zn(1) and Zn(2) atoms form binuclear ‘paddlewheel’ blocks $\{\text{Zn}_2(\text{OOCR})_4\}$ interconnected by four sedc^{2-} anions into square-grid network. The angular shape of the sedc^{2-} ligands results in a considerable distortion of the binuclear blocks (Figure 1a) and corrugation of the square-grid layers (Figure 1b). These layers are bound by dabco bridges to form a three-dimensional porous framework with a primitive cubic topology (**pcu**)—the same as the other MOFs of the isorecticular family $[\text{Zn}_2(\text{bdc})_2(\text{dabco})]$.

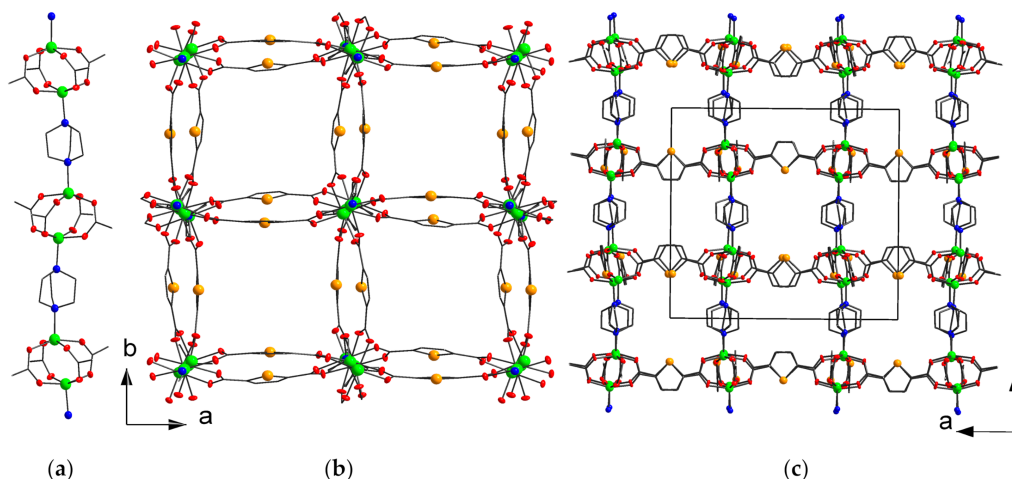


Figure 1. Crystal structure of **1se**. A section of the structure showing dabco-bridged secondary building units $\{Zn_2(OOCR)_4\}$ (a); 3D structure of the framework: view along c axis (b) and b axis (c). Zn atoms are shown green, N atoms—blue, O atoms—red, Se atoms—orange. H atoms and guest DMF molecules are not shown.

The coordination network in **1se** contains a three-dimensional system of intersecting channels, with the widest channels running along the c axis, across the windows of the square-grid layers (see Figure 1b). The apertures of these channels are $5 \times 8 \text{ \AA}$. Two different types of smaller channels across the main channels of the tetragonal structure have smaller the apertures of ca. $2.5 \times 5 \text{ \AA}$ or $3.5 \times 4 \text{ \AA}$, depending on the particular arrangement of arks of the $sedc^{2-}$ ligands (Figure 1c). Importantly, all selenium atoms of the heterocycles are immediately accessible for interactions with potential substrate molecules, allowing a clear verification of the hypothesis of this work. We should also point out that the crystal structure **1se** is similar to the known compound $[Zn_2(tdc)_2(dabco)]$ (**1t**), based on 2,5-thiophenedicarboxylate [31] although the distortions of the binuclear blocks $\{Zn_2(OOCR)_4\}$ and the square-grid layers in **1t** are even more pronounced as a result of stronger bending of tdc^{2-} ligand [34], compared with that of $sedc^{2-}$.

2.2. Characterization and Activation

To evaluate the thermal stability of **1se**, thermogravimetric analysis (TGA, Figure S1) was performed. The first observed 30% weight loss step occurs between $80 \text{ }^\circ\text{C}$ and $200 \text{ }^\circ\text{C}$, referring to the evaporation of four guest DMF molecules per formula unit (calculated: 30%). The metal–organic framework **1se** itself is stable up to ca. $280 \text{ }^\circ\text{C}$, after which the irreversible framework decomposition apparently takes place. Such thermal stability is comparable to other reported MOFs containing $sedc^{2-}$ anions ($T_{decomp} = 250 \div 320 \text{ }^\circ\text{C}$) [32,33]. Such substantial difference between the temperature of the evaporation of guests and the temperature of the framework decomposition makes it possible direct activation of **1se** by heating in a vacuum, obtaining the guest-free activated framework $[Zn_2(sedc)_2(dabco)]$ (**1se'**). The infrared spectra of both **1se** and **1se'** (Figure S2) contain the characteristic bands of Csp^2 -H valence vibrations (3073 cm^{-1}), Csp^3 -H valence vibrations (2965 cm^{-1} and 2935 cm^{-1}), antisymmetric (1590 cm^{-1}) and symmetric (1360 cm^{-1}) carboxylate group vibrations. Infrared spectrum of **1se** also contains a characteristic band of CO_{amide} stretchings (1666 cm^{-1}), which is absent on the spectrum of **1se'**, confirming a complete desolvation of metal–organic framework **1se** during the activation process. The PXRD data (Figure 2) suggest the phase purity of the synthesized compound **1se**. The powder diffraction pattern of **1se'** is generally very similar to that of **1se** although there is a noticeable shift of some of the reflexes to lower angles. For example, the $(2\ 0\ 0)$ reflection at $2\theta = 8.57^\circ$ (**1se**) is shifted to $2\theta = 8.36^\circ$ (**1se'**) indicating a slight extension of the metal–organic framework upon its activation. Similar guest-assisted breathing of the framework was observed earlier for **1b** and **1t** [31,35]. The unit cell parameters for **1se'** were refined according to the powder data using

the Powdercell program [36] and provided in Table A2. While the crystallographic parameter c is almost intact, the parameters a and b in **1se'** are longer by ca. 2.6% than in **1se**, likely due to certain straightening of the sedc^{2-} dicarboxylate bridges. Overall, the unit cell volume is expanded by 5.2% during the activation of the compound.

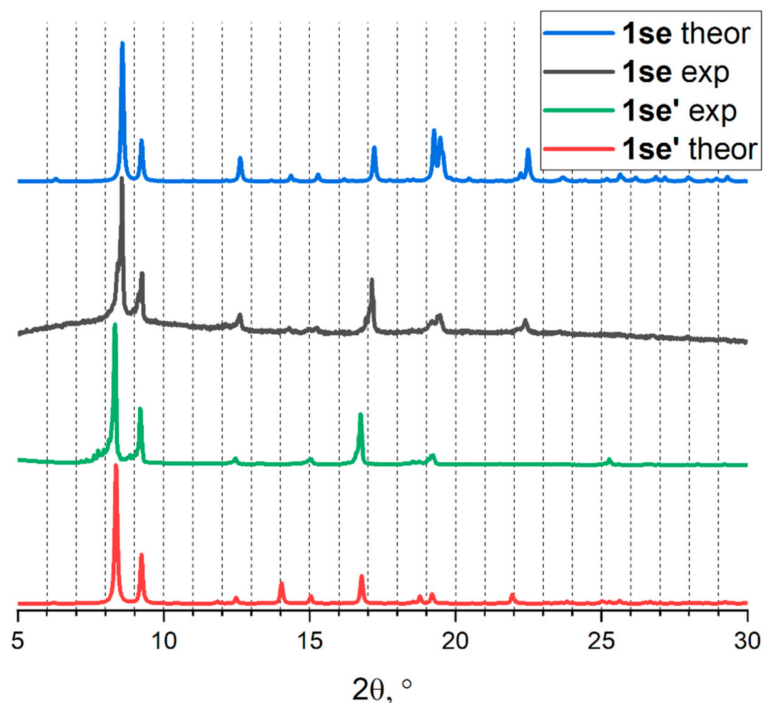


Figure 2. PXRD patterns of the theoretically simulated **1se** (blue), as-synthesized **1se** (black), activated **1se'** (olive), and the theoretically simulated **1se'** (red), assuming the retention of the space group $P-42_1c$.

2.3. Adsorption Measurements

The textural characteristics of the evacuated compound **1se'** were studied by a nitrogen porosimetry at 77 K. The adsorption isotherm (Figure 3) corresponds to the type I with no hysteresis, typical to microporous adsorbents. The pore volume measured at $p/p^0 = 0.95$ is $V_{\text{pore}} = 0.57 \text{ cm}^3 \cdot \text{g}^{-1}$; the calculated BET surface area is $A_{\text{BET}} = 1504 \text{ m}^2 \cdot \text{g}^{-1}$, respectively (see other details in Table S1). The experimental V_{pore} is very much consistent with the theoretically expected value based on a solvent accessible volume of **1se'**, calculated using PLATON routine [37] ($0.58 \text{ cm}^3 \cdot \text{cm}^{-3}$ or $0.55 \text{ cm}^3 \cdot \text{g}^{-1}$). The pore-size distribution, calculated by DFT method from the N_2 adsorption isotherm, gives a value of a pore size near 7 Å, which corresponds to the van der Waals diameter of the large cuboidal cages inside the **pcu** net. For a reference, the pore volume of the activated MOFs based on thiophenedicarboxylic acid (**1t'**) or benzenedicarboxylic acid (**1b'**), reported earlier, are $0.68 \text{ cm}^3 \cdot \text{g}^{-1}$ and $0.75 \text{ cm}^3 \cdot \text{g}^{-1}$, respectively. The gravimetric porosity directly depends on molecular weight of a compound, which is notably higher for **1se**, than for **1t** and **1b**. The comparison of experimental volumetric porosities for these MOFs results in a more or less comparable values: $0.60 \text{ cm}^3 \cdot \text{cm}^{-3}$ (**1se'**), $0.64 \text{ cm}^3 \cdot \text{cm}^{-3}$ (**1t'**), $0.62 \text{ cm}^3 \cdot \text{cm}^{-3}$ (**1b'**), see also Table S2. Most importantly, the compounds **1b**, **1t**, and **1se** represent a suitable family of porous materials where the influence of different heteroatoms on the gas adsorption properties could be systematically analyzed and assessed since the other parameters are almost identical. Being motivated by such an opportunity, we investigated the adsorption properties of **1se'** towards industrially important gases (CO_2 and CH_4) and compared the obtained data with the other prototypes **1b'** and **1t'**.

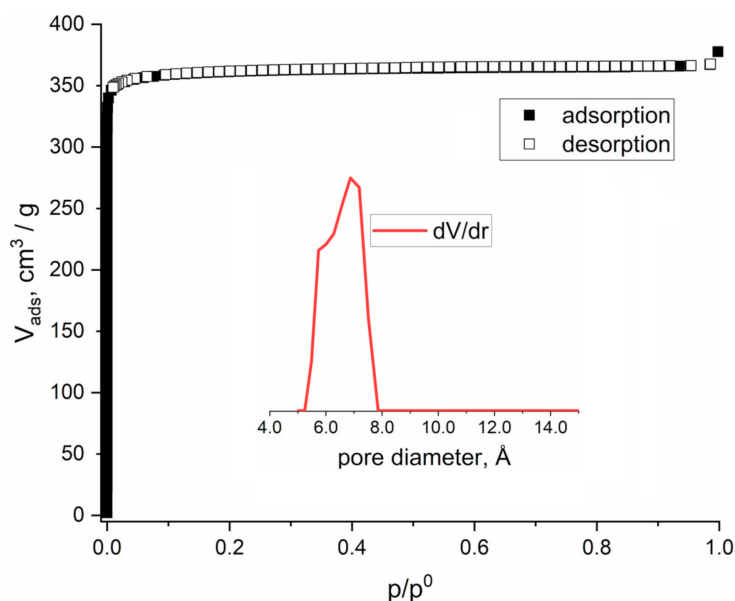


Figure 3. N₂ adsorption isotherm for **1se'** at 77K and pore-size distribution calculated from the isotherm.

The gravimetric CO₂ adsorption uptakes at 1 bar for **1se'** are 110 cm³·g⁻¹ (273 K, see Figure S3) and 46 cm³·g⁻¹ (298 K). Such numbers are comparable with the literature data of CO₂ adsorption by **1b'** (122 cm³·g⁻¹ at 273 K, 46 cm³·g⁻¹ at 298 K). Taking into account the crystallographic densities, the corresponding volumetric uptakes for **1se'** were calculated to be 116 cm³·cm⁻³ (273 K) and 48.5 cm³·cm⁻³ (298 K), which exceeds those for **1b'** by 15% (101 cm³·cm⁻³) at 273 K (see Figure 4) and by 28% (38 cm³·cm⁻³) at 298 K, respectively, convincingly confirming a positive effect of the polarizable heteroatom (Se) on the absorption properties of porous materials [38–41]. Similarly, the isosteric heat of CO₂ adsorption at zero coverage $Q_{st}(0)$ for **1se'** (19.9 kJ·mol⁻¹) is greater than for **1b'** (19.0 kJ·mol⁻¹), indicating stronger binding of CO₂ with the porous framework containing the selenophene heterocycle. We must mention here that the CO₂ adsorption by **1t'** is still the highest among the MOFs discussed here, both in terms of the gravimetric uptakes (153 cm³·g⁻¹ at 273 K, 67.5 cm³·g⁻¹ at 298 K, 1 bar) and volumetric uptakes (143 cm³·cm⁻³ at 273 K, 63.1 cm³·cm⁻³ at 298 K, 1 bar). The isosteric heat of CO₂ adsorption by **1t'** (23.7 kJ·mol⁻¹) also suggests that the thiophene moieties have greater impact on the CO₂ adsorption. It is probably the polarity of the aromatic ring that contributes to a stronger binding between the polar CO₂ guest and porous MOF host. Based on the experimental data, the following dependence of the CO₂ uptake on the nature of the dicarboxylate anion was established: tdc²⁻ > sedc²⁻ > bdc²⁻. This dependence strengthens the earlier claim that the substitution of the common terephthalate linkers to heterocyclic ones should enhance the adsorption properties of the MOF material due to induced dipole interactions. In terms of the gas storage, the thiophene-containing tdc²⁻ seems to be an optimal choice for such substitution since the incorporation of heavier sedc²⁻ no longer improves the gas adsorption capacity of the framework.

The CH₄ and N₂ adsorption–desorption isotherms for **1se'** and **1b'** were measured up to $p = 1$ bar at 273 K. The gas adsorption isotherms are shown on the Figure 5. For **1se'** the gravimetric adsorption volumes at 1 bar are 16.2 cm³·g⁻¹ (CH₄) and 6.0 cm³·g⁻¹ (N₂) adsorption, respectively. For **1b'**, the corresponding uptakes are 20.0 cm³·g⁻¹ and 6.6 cm³·g⁻¹. The gravimetric gas uptakes for **1se'** are slightly lower than for **1b'**, mainly due to the higher density of the former. On the contrary, the volumetric assessment indicates higher gas adsorption by **1se'**, than by **1b'**, supporting the concept of stronger van der Waals interactions of methane/nitrogen with sedc²⁻ than with bdc²⁻.

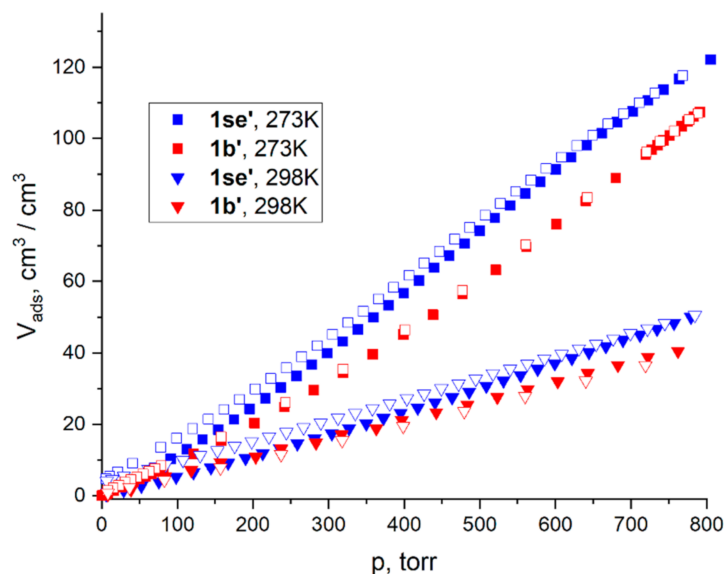


Figure 4. Volumetric CO₂ sorption isotherms for **1se'** and **1b'** at 273 K and 298 K.

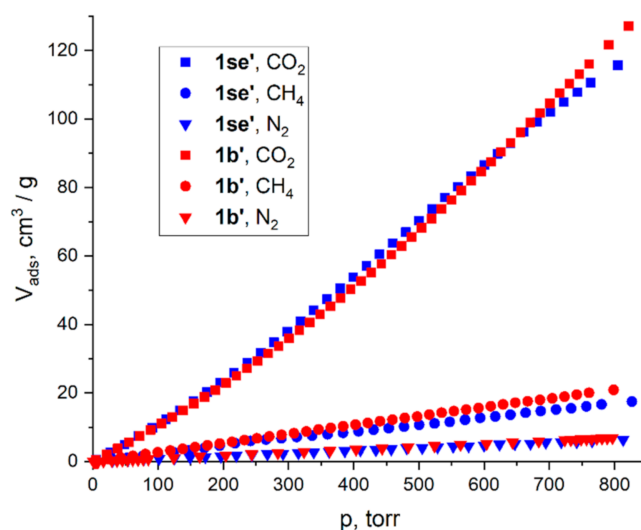


Figure 5. Gravimetric CO₂, CH₄, and N₂ sorption isotherms for **1se'** and **1b'** (b) at 273 K. Only adsorption branches are shown.

The sequestration of CO₂ from N₂ or from CH₄ is a critical technology for a reduction of environmental risks and for protection of natural gas pipelines, respectively. The CO₂/CH₄ as well as CO₂/N₂ gas adsorption selectivity factors were calculated by three commonly employed approaches: (i) as the ratio of the adsorbed volumes at 1 bar (S_V), (ii) as the ratio of Henry constants (S_K), and (iii) by the ideal adsorbate solution theory (S_{IAST}). The calculated selectivity values are summarized in Table 1, and the details of the calculations are provided in Tables S3 and S4. By any criteria used, the incorporation of sedc²⁻ evidently increases the adsorption selectivities of **1se'**, compared with the prototypic **1b'**. The calculated CO₂/CH₄ selectivity factors for **1se'** ($S_V = 6.8$, $S_K = 4.8$, $S_{IAST} = 5.6$) are comparable or even exceed those reported for other MOFs with promising application potential for separation of such small molecules [42–44]. The CO₂/N₂ adsorption selectivity factors for **1se'** are also quite remarkable $S_V = 18.6$, $S_K = 12.9$, $S_{IAST} = 15.1$ (Figure 6) for a porous MOF with no unsaturated metal centers. The results obtained for **1se'** are superior to the CO₂/N₂ selectivity factors for both **1b'** and **1t'**. Particularly, the IAST CO₂ adsorption selectivity for the equimolar CO₂ + N₂ gas mixture for **1se'** is ca. 25% greater than for **1b'** or for **1t'** (see also Figure S4). Such remarkable increase should

apparently be attributed to the nature of the heterocyclic moiety since the pore geometry and other structural parameters of the investigated MOFs are, essentially, the same. However, the contribution of sieving effect is also possible, as the channels in **1se** situated along two of three directions have the apertures smaller than 5 Å [45,46]. In terms of the CO₂/N₂ selective separation, the incorporation of the selenophene-containing anion provides the best performance in the row: sedc²⁻ > tdc²⁻ > bdc²⁻. Moreover, a rather low CO₂ adsorption enthalpy for **1se'** (19.9 kJ·mol⁻¹) ensures the facile regeneration of the porous adsorbent in a cyclic CO₂ sequestration process. The unique combination of remarkable CO₂/N₂ adsorption selectivity, high CO₂ uptake, and one of the lowest CO₂ adsorption enthalpies puts the title MOF **1se'** among the best porous materials for practical purification of the industrial exhausts.

Table 1. Selectivities in binary gas mixtures calculated (I) as volumes ratio at 1 bar (II) as Henry constants ratio and (III) IAST selectivity factors for equimolar mixtures at 1 bar.

Gas Mixture	V ₁ /V ₂ (273 K, 1 Bar)			K _{h1} /K _{h2} (273 K)			IAST (273 K, 50:50 Ratio)		
	1se	1t	1b	1se	1t	1b	1se	1t	1b
CO ₂ /N ₂ (in this work)	18.6	–	17.7	12.9	–	11.8	15.1	–	11.9
CO ₂ /N ₂ (from Ref. [29])	–	10.3	18.8	–	12.5	8.9	–	11.2	9.2
CO ₂ /CH ₄ (in this work)	6.8	–	5.8	4.8	–	3.9	5.6	–	4.1

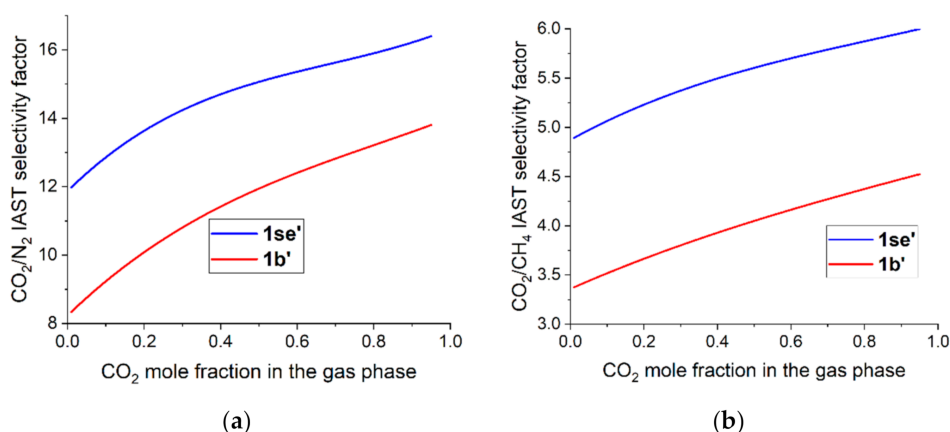


Figure 6. IAST selectivity factors on CO₂ mole fraction in binary gas mixtures: CO₂/N₂ (a) and CO₂/CH₄ (b) at 273K and $P_{\text{total}} = 1$ bar.

3. Materials and Methods

4. Reagents

Commercial starting reagents 2,5-selenophenedicarboxylic acid (Angene), 1,4-diazabicyclo[2.2.2]octane (>98.0%, TCI), terephthalic acid (>98.0%, Hidmon), *N,N*-dimethylformamide (reagent grade, Vekton) were used as purchased without purification.

5. Instruments

IR spectra in KBr pellets were recorded in the range 4000–400 cm⁻¹ on a VERTEX 80 spectrometer. Elemental (C, H, N) analysis was made on a varioMICROcube analyzer. Powder X-ray diffraction (PXRD) analysis was performed at room temperature on a Shimadzu XRD-7000 diffractometer (Cu-K α radiation, $\lambda = 1.54178$ Å). Thermogravimetric analysis was carried out on a Netzsch TG 209 F1 Iris instrument. The experiments were carried out under He flow (30 cm³·min⁻¹) at a 10 K·min⁻¹ heating rate. Adsorption experiments were performed using Quantachrome Autosorb iQ device.

Low-pressure gas adsorption isotherms at 273 K and 298 K were recorded with a thermostat TERMEX Cryo-VT-12 to adjust temperature with 0.1 K accuracy. The database of the National Institute of Standards and Technology was used as a source of p - V - T relations at experimental pressures and temperatures. Elemental (Zn, Se) ICP-MS analysis was carried out using Agilent 8800. The samples of **1se** and **1se'** were digested in the mixture of HCl 36% water solution and H₂O₂ 30% water solution, then diluted by water prior to ICP-MS.

6. X-ray Crystallography

Diffraction data for single-crystal **1se** were obtained at 130 K on an automated Agilent Xcalibur diffractometer equipped with an area AtlasS2 detector (graphite monochromator, $\lambda(\text{MoK}\alpha) = 0.71073 \text{ \AA}$, ω -scans with a step of 0.5°). Integration, absorption correction, and determination of unit cell parameters were performed using the CrysAlisPro program package [47]. The structures were solved by dual space algorithm (SHELXT [48]) and refined by the full-matrix least squares technique (SHELXL [49]) in the anisotropic approximation (except hydrogen atoms). Positions of hydrogen atoms were calculated geometrically and refined in the riding model. The crystallographic data and details of the structure refinement are summarized in Table A1. CCDC 2026693 contains the supplementary crystallographic data for this paper. These data can be obtained free of charge from The Cambridge Crystallographic Data Center at <https://www.ccdc.cam.ac.uk/structures/>.

7. Synthetic Procedures

Synthesis of $[\text{Zn}_2(\text{sedc})_2(\text{dabco})]\cdot 4\text{DMF}$ (**1se**) 100 mg (0.34 mmol) of $\text{Zn}(\text{NO}_3)_2\cdot 6\text{H}_2\text{O}$, 66 mg (0.30 mmol) of H₂sedc, 20 mg (0.18 mmol) of dabco and 5.00 mL of DMF were mixed in a glass flask. The mixture was hit in the ultrasound bath for 10 min and heated at 100 °C for 24 h. After the cooling to the room temperature white-yellow precipitate was filtered off, washed thrice with DMF and dried in air. Yield: 89 mg (61%). IR spectrum (KBr, cm^{-1}) characteristic bands: 3424 (w, br, νOH); 3073 (w, $\nu\text{Csp}^2\text{-H}$); 2965 and 2925 (w, $\nu\text{Csp}^3\text{-H}$); 1666 (s, $\nu\text{CO}_{\text{amide}}$); 1627 (m, $\nu\text{COO}_{\text{as}}$); 1380 (s, νCOO_{s}). PXRD data (Figure 2) confirmed the phase purity of the product. Elemental analysis data calculated for $[\text{Zn}_2(\text{C}_6\text{H}_2\text{SeO}_4)_2(\text{C}_6\text{H}_{12}\text{N}_2)]\cdot 4\text{C}_3\text{H}_7\text{NO}$ (%): C, 37.2; H, 4.6; N, 8.7. Found (%): C, 37.0; H, 4.6; N, 8.6. ICP-MS data. Zn:Se molar ratio: 1.02: 1 (theor = 1:1). TGA: 30% weight loss step at ca.150 °C (30% calculated for 4DMF).

Synthesis of $[\text{Zn}_2(\text{sedc})_2(\text{dabco})]$ (**1se'**) The sample of **1** was activated by keeping in a primary vacuum (10^{-9} bar) at 50 °C for 2 h, then at 70 °C for 2 h, and at last 90 °C for 12 h with $1^\circ\cdot\text{min}^{-1}$ heating and cooling rates. IR spectrum (KBr, cm^{-1}) characteristic bands: 3419 (w, br, νOH); 3075 (w, $\nu\text{Csp}^2\text{-H}$); 2963 and 2926 (w, $\nu\text{Csp}^3\text{-H}$); 1585 (m, $\nu\text{COO}_{\text{as}}$); 1356 (s, νCOO_{s}). PXRD data (Figure 2) confirmed the phase purity of the product. Elemental analysis data calculated for $[\text{Zn}_2(\text{C}_6\text{H}_2\text{SeO}_4)_2(\text{C}_6\text{H}_{12}\text{N}_2)]$ (%): C, 31.9; H, 2.4; N, 4.1. Found (%): C, 31.8; H, 2.5; N, 4.5. ICP-MS data. Zn:Se molar ratio: 1.07: 1 (theor = 1:1).

Synthesis of $[\text{Zn}_2(\text{bdc})_2(\text{dabco})]\cdot \frac{1}{2}\text{H}_2\text{O}$ (**1b**) This process carried out according to the published procedure [50]: 300 mg (1.0 mmol) of $\text{Zn}(\text{NO}_3)_2\cdot 6\text{H}_2\text{O}$, 165 mg (1.0 mmol) of H₂bdc, 60 mg (0.54 mmol) of dabco and 18.0 mL of DMF were mixed in a glass flask. The mixture was hit in the ultrasound bath for 10 min and heated at 120 °C for 48 h. After the cooling to the room temperature white precipitate was filtered off, washed thrice with DMF and dried in air. Yield: 380 mg (88%). PXRD data (Figure S5) confirmed the phase purity of the product.

Synthesis of $[\text{Zn}_2(\text{bdc})_2(\text{dabco})]$ (**1b'**) The sample of **1b** was activated by keeping in a primary vacuum (10^{-9} bar) at 50 °C for 2 h, then at 80 °C for 2 h, and at 100 °C for 12 h with $1^\circ\cdot\text{min}^{-1}$ heating and cooling rates. PXRD data (Figure S6) confirmed the phase purity of the product.

8. Conclusions

To summarize, a new porous metal-organic framework $[\text{Zn}_2(\text{sedc})_2(\text{dabco})]$, based on 2,5-selenophenedicarboxylate anions (sedc^{2-}) was synthesized and characterized. $[\text{Zn}_2(\text{sedc})_2(\text{dabco})]$

is based on the $\{Zn_2(OOCR)_4N_2\}$ paddle-wheel blocks and adopts distorted primitive cubic topology, similar to other important representatives of this isorecticular family $[Zn_2(bdc)_2(dabco)]$ and $[Zn_2(tdc)_2(dabco)]$ ($bdc^{2-} = 1,4$ -benzenedicarboxylate, $tdc^{2-} = 2,5$ -thiophenedicarboxylate). The dependence of the gas adsorption properties on the nature of the bridging anion was systematically investigated. According to the experimental and literature data, the CO_2 adsorption uptake increases along the following sequence: $[Zn_2(bdc)_2(dabco)] < [Zn_2(secdc)_2(dabco)] < [Zn_2(tdc)_2(dabco)]$. On the other hand, the CO_2/N_2 adsorption selectivity follows the trend $[Zn_2(bdc)_2(dabco)] < [Zn_2(tdc)_2(dabco)] < [Zn_2(secdc)_2(dabco)]$. Such dependencies strengthen the earlier observation that the incorporation of heterocyclic moieties provides additional adsorption sites which enhances the adsorption properties of the corresponding porous frameworks. The selenophene-based anion seems to have a particular distinction towards CO_2 molecules. The new porous compound $[Zn_2(secdc)_2(dabco)]$ features a unique combination of remarkable CO_2/N_2 adsorption selectivity, high CO_2 uptake, and one of the lowest CO_2 adsorption enthalpies, which makes it a very promising material for CO_2 sequestration applications.

Supplementary Materials: The following are available online. Figure S1: TG plot of the synthesized **1se**; Figure S2: IR spectra of the synthesized **1se** and activated **1se'**; Figure S3: Gravimetric CO_2 , CH_4 and N_2 sorption isotherms for **1se'** (a) and **1b'** (b) at 273 K; Figure S4: Dependences of adsorbed CO_2 mole fraction in MOF on CO_2 mole fraction in gas phase for binary gas mixtures: CO_2/N_2 and CO_2/CH_4 at 273K and $P_{total} = 1$ bar; Figure S5: PXRD pattern of the synthesized compound **1b** compared to the theoretical one; Figure S6: PXRD pattern of the synthesized compound **1b'** compared to the theoretical one for **1b'**; Table S1: Textural characteristics of **1se'**; Table S2: Calculated virial coefficients for CO_2 isosteric heats of adsorption and Henry constants determination; Table S3: Fit parameters of the isotherms for IAST calculations.

Author Contributions: P.A.D., S.S.V., and D.G.S. performed the experimental work. P.A.D. prepared the original manuscript. D.N.D. and V.P.F. reviewed and edited the manuscript. D.N.D. project administration and funding acquisition. All authors have read and agreed to the published version of the manuscript.

Funding: This work was supported by Russian Science Foundation, project no. 18-13-00203.

Conflicts of Interest: The authors declare no conflict of interest.

Appendix A Crystallographic data

Table A1. Crystal data and structure refinement for **1se**.

Identification Code	1se
CCDC Number	2026693
Empirical formula	$C_{30}H_{44}N_6O_{12}Se_2Zn_2$
<i>M</i> , g/mol	969.37
Crystal system	Tetragonal
Space group	$P-42_1c$
<i>a</i> , <i>b</i> , Å	20.59224(17)
<i>c</i> , Å	19.1260(2)
<i>V</i> , Å ³	8110.20(16)
<i>Z</i>	8
<i>D</i> (calc.), g/cm ³	1.588
μ , mm ⁻¹	3.040
<i>F</i> (000)	3920
Crystal size, mm	0.36 × 0.26 × 0.20
θ range for data collection, deg.	1.98–28.28
Index ranges	$-27 \leq h \leq 19, -22 \leq k \leq 25, -22 \leq l \leq 25$
Reflections collected/independent	24,964 8741
R_{int}	0.0225
Reflections with $I > 2\sigma(I)$	8293
Goodness-of-fit on F^2	1.044
Final <i>R</i> indices [$I > 2\sigma(I)$]	$R_1 = 0.0223, wR_2 = 0.0492$
<i>R</i> indices (all data)	$R_1 = 0.0253, wR_2 = 0.0502$
Largest diff. peak/hole, e/Å ³	0.397/−0.271

Table A2. Refined unit cell parameters for **1se'**.

Identification Code	1se'
Crystal System	Tetragonal
a, b, Å	21.1165
c, Å	19.1304
V, Å ³	8530.5
D(calc.), g/cm ³	1.055

References

- Dutcher, B.; Fan, M.; Russell, A.G. Amine-Based CO₂ Capture Technology Development from the Beginning of 2013—A Review. *ACS Appl. Mater. Interfaces* **2015**, *7*, 2137–2148. [[CrossRef](#)] [[PubMed](#)]
- Wang, J.; Huang, L.; Yang, R.; Zhang, Z.; Wu, J.; Gao, Y.; Wang, Q.; O'Hareb, D.; Zhong, Z. Recent advances in solid sorbents for CO₂ capture and new development trends. *Energy Environ. Sci.* **2014**, *7*, 3478–3518. [[CrossRef](#)]
- Bhattacharyya, D.; Miller, D.C. Post-combustion CO₂ capture technologies—A review of processes for solvent-based and sorbent-based CO₂ capture. *Curr. Opin. Chem. Eng.* **2017**, *17*, 78–92. [[CrossRef](#)]
- Leung, D.Y.C.; Caramanna, G.; Mercedes Maroto-Valer, M. An overview of current status of carbon dioxide capture and storage technologies. *Renew. Sustain. Energy Rev.* **2014**, *39*, 426–443. [[CrossRef](#)]
- Lin, R.B.; Li, L.; Alsalmeh, A.; Chen, B. An Ultramicroporous Metal–Organic Framework for Sieving Separation of Carbon Dioxide from Methane. *Small Struct.* **2020**. [[CrossRef](#)]
- Ding, M.; Flaig, R.W.; Jiang, H.-L.; Yaghi, O.M. Carbon capture and conversion using metal–organic frameworks and MOF-based materials. *Chem. Soc. Rev.* **2019**, *48*, 2783–2828. [[CrossRef](#)] [[PubMed](#)]
- Zhang, Z.; Yao, Z.-Z.; Xiang, S.; Chen, B. Perspective of microporous metal–organic frameworks for CO₂ capture and separation. *Energy Environ. Sci.* **2014**, *7*, 2868–2899. [[CrossRef](#)]
- Siegelman, R.L.; Milner, P.J.; Forse, A.C.; Lee, J.-H.; Colwell, K.A.; Neaton, J.B.; Reimer, J.A.; Weston, S.C.; Long, J.R. Water Enables Efficient CO₂ Capture from Natural Gas Flue Emissions in an Oxidation-Resistant Diamine-Appended Metal–Organic Framework. *J. Am. Chem. Soc.* **2019**, *141*, 13171–13186. [[CrossRef](#)]
- Lin, Y.; Kong, C.; Zhang, Q.; Chen, L. Metal–Organic Frameworks for Carbon Dioxide Capture and Methane Storage. *Adv. Energy Mater.* **2017**, *7*, 1601296. [[CrossRef](#)]
- Belmabkhout, Y.; Guillerm, V.; Eddaoudi, M. Low concentration CO₂ capture using physical adsorbents: Are metal-organic frameworks becoming the new benchmark materials? *Chem. Eng. J.* **2016**, *296*, 386–397. [[CrossRef](#)]
- Eddaoudi, M.; Kim, J.; Rosi, N.; Vodak, D.; Wachter, J.; O'Keeffe, M.; Yaghi, O.M. Systematic Design of Pore Size and Functionality in Isoreticular MOFs and Their Application in Methane Storage. *Science* **2002**, *295*, 469–472. [[CrossRef](#)]
- Guo, P.; Dutta, P.; Wong-Foy, A.G.; Gidley, D.W.; Matzger, A.J. Water Sensitivity in Zn₄O-Based MOFs is Structure and History Dependent. *J. Am. Chem. Soc.* **2015**, *137*, 2651–2657. [[CrossRef](#)] [[PubMed](#)]
- Zhou, H.-F.; Liu, B.; Hou, L.; Zhang, W.-Y.; Wang, Y.-Y. Rational construction of a stable Zn₄O-based MOF for highly efficient CO₂ capture and conversion. *Chem. Commun.* **2018**, *54*, 456–459. [[CrossRef](#)] [[PubMed](#)]
- Loiseau, T.; Serre, C.; Huguenard, C.; Fink, G.; Taulelle, F.; Henry, M.; Bataille, T.; Férey, G. A rationale for the large breathing of the porous aluminum terephthalate (MIL-53) upon hydration. *Chem. Eur. J.* **2004**, *10*, 1373–1382. [[CrossRef](#)]
- Senkowska, I.; Hoffmann, F.; Fröba, M.; Getzschmann, J.; Böhlmann, W.; Kaskel, S. New highly porous aluminium based metal-organic frameworks: Al(OH)(ndc) (ndc = 2,6-naphthalene dicarboxylate) and Al(OH)(bpdc) (bpdc = 4,4'-biphenyl dicarboxylate). *Microporous Mesoporous Mater.* **2009**, *122*, 93–98. [[CrossRef](#)]
- Rabe, T.; Pewe, H.; Reinsch, H.; Willhammar, T.; Svensson Grape, E.; Stock, N. Influence of the substitution pattern of four naphthalenedicarboxylic acids on the structures and properties of group 13 metal-organic frameworks and coordination polymers. *Dalton Trans.* **2020**, *49*, 4861–4868. [[CrossRef](#)] [[PubMed](#)]

17. Cavka, J.H.; Jakobsen, S.; Olsbye, U.; Guillou, N.; Lamberti, C.; Bordiga, S.; Lillerud, K.P. A New Zirconium Inorganic Building Brick Forming Metal Organic Frameworks with Exceptional Stability. *J. Am. Chem. Soc.* **2008**, *130*, 13850–13851. [[CrossRef](#)]
18. Lammert, M.; Wharmby, M.; Smolders, S.; Bueken, B.; Lieb, A.; Lomachenko, K.A.; De Vos, D.; Stock, N. Cerium-based metal organic frameworks with UiO-66 architecture: Synthesis, properties and redox catalytic activity. *Chem. Commun.* **2015**, *51*, 12578–12581. [[CrossRef](#)]
19. Waitschat, S.; Fröhlich, D.; Reinsch, H.; Terraschke, H.; Lomachenko, K.A.; Lamberti, C.; Kummer, H.; Helling, T.; Baumgartner, M.; Henninger, S.; et al. Synthesis of M-UiO-66 (M = Zr, Ce or Hf) employing 2,5-pyridinedicarboxylic acid as a linker: Defect chemistry, framework hydrophilisation and sorption properties. *Dalton Trans.* **2018**, *47*, 1062–1070. [[CrossRef](#)]
20. Wang, H.; Wen, R.-M.; Hu, T.-L. Two Series of Lanthanide Metal-Organic Frameworks Constructed from Crown-Ether-Like Secondary Building Units. *Eur. J. Inorg. Chem.* **2014**, *2014*, 1185–1191. [[CrossRef](#)]
21. Sapchenko, S.A.; Demakov, P.A.; Samsonenko, D.G.; Dybtsev, D.N.; Schröder, M.; Fedin, V.P. A Cryptand Metal–Organic Framework as a Platform for the Selective Uptake and Detection of Group I Metal Cations. *Chem. Eur. J.* **2017**, *23*, 2286–2289. [[CrossRef](#)] [[PubMed](#)]
22. Chen, S.; Feng, F.; Li, S.; Li, X.-X.; Shu, L. Metal-organic framework DUT-67 (Zr) for adsorptive removal of trace Hg²⁺ and CH₃Hg⁺ in water. *Chem. Speciat. Bioavailab.* **2018**, *30*, 99–106. [[CrossRef](#)]
23. Chen, Q.; Guo, P.-C.; Zhao, S.-P.; Liu, J.-L.; Ren, X.-M. A rhombus channel metal–organic framework comprised of Sr²⁺ and thiophene-2,5-dicarboxylic acid exhibiting novel dielectric bistability. *CrystEngComm* **2013**, *15*, 1264–1270. [[CrossRef](#)]
24. Dreischarf, A.C.; Lammert, M.; Stock, N.; Reinsch, H. Green Synthesis of Zr-CAU-28: Structure and Properties of the First Zr-MOF Based on 2,5-Furandicarboxylic Acid. *Inorg. Chem.* **2017**, *56*, 2270–2277. [[CrossRef](#)]
25. Lysova, A.A.; Samsonenko, D.G.; Dorovatovskii, P.V.; Lazarenko, V.A.; Khrustalev, V.N.; Kovalenko, K.A.; Dybtsev, D.N.; Fedin, V.P. Tuning the Molecular and Cationic Affinity in a Series of Multifunctional Metal–Organic Frameworks Based on Dodecanuclear Zn(II) Carboxylate Wheels. *J. Am. Chem. Soc.* **2019**, *141*, 17260–17269. [[CrossRef](#)]
26. Petkov, P.S.; Bon, V.; Hobday, C.L.; Kuc, A.B.; Melix, P.; Kaskel, S.; Düren, T.; Heine, T. Conformational isomerism controls collective flexibility in metal–organic framework DUT-8(Ni). *Phys. Chem. Chem. Phys.* **2019**, *21*, 674–680. [[CrossRef](#)] [[PubMed](#)]
27. Chun, H.; Dybtsev, D.N.; Kim, H.; Kim, K. Synthesis, X-ray crystal structures, and gas sorption properties of pillared square grid nets based on paddle-wheel motifs: Implications for hydrogen storage in porous materials. *Chem. Eur. J.* **2005**, *11*, 3521–3529. [[CrossRef](#)]
28. Dybtsev, D.N.; Yutkin, M.P.; Peresypkina, E.V.; Virovets, A.V.; Serre, C.; Férey, G.; Fedin, V.P. Isoreticular homochiral porous metal-organic structures with tunable pore sizes. *Inorg. Chem.* **2007**, *46*, 6843–6845. [[CrossRef](#)]
29. Khan, I.S.; Samsonenko, D.G.; Irgashev, R.A.; Kazin, N.A.; Rusinov, G.L.; Charushin, V.N.; Zavakhina, M.S.; Fedin, V.P. Synthesis, crystal structure and fluorescent properties of indolo[3,2-b]carbazole-based metal–organic coordination polymers. *Polyhedron* **2017**, *141*, 337–342. [[CrossRef](#)]
30. Cheplakova, A.M.; Kovalenko, K.A.; Samsonenko, D.G.; Lazarenko, V.A.; Khrustalev, V.N.; Vinogradov, A.S.; Karpov, V.M.; Platonov, V.E.; Fedin, V.P. Metal-organic frameworks based on octafluorobiphenyl-4, 4'-dicarboxylate: Synthesis, crystal structure, and surface functionality. *Dalton Trans.* **2018**, *47*, 3283–3297. [[CrossRef](#)]
31. Bolotov, V.A.; Kovalenko, K.A.; Samsonenko, D.G.; Han, X.; Zhang, X.; Smith, G.L.; McCormick, L.J.; Teat, S.J.; Yang, S.; Lennox, M.J.; et al. Enhancement of CO₂ Uptake and Selectivity in a Metal–Organic Framework by the Incorporation of Thiophene Functionality. *Inorg. Chem.* **2018**, *57*, 5074–5082. [[CrossRef](#)] [[PubMed](#)]
32. Hua, C.; D'Alessandro, D.M. Systematic Tuning of Zn(II) frameworks with Furan, Thiophene and Selenophene Dipyridyl and Dicarboxylate Ligands. *Cryst. Growth Des.* **2017**, *17*, 6262–6272. [[CrossRef](#)]
33. Ding, B.; Hua, C.; Kepert, C.J.; D'Alessandro, D.M. Influence of structure–activity relationships on through-space intervalence charge transfer in metal–organic frameworks with cofacial redox-active units. *Chem. Sci.* **2019**, *10*, 1392–1400. [[CrossRef](#)] [[PubMed](#)]
34. Lysova, A.; Samsonenko, D.; Dybtsev, D.; Fedin, V. Synthesis and luminescence properties of new metal-organic frameworks based on zinc(II) ions and 2,5-thiophenedicarboxylate ligands. *Crystals* **2018**, *8*, 7. [[CrossRef](#)]

35. Dybtsev, D.N.; Chun, H.; Kim, K. Rigid and Flexible: A Highly Porous Metal–Organic Framework with Unusual Guest-Dependent Dynamic Behavior. *Angew. Chem. Int. Ed.* **2004**, *43*, 5033–5036. [[CrossRef](#)]
36. Kraus, W.; Nolze, G. POWDER CELL—A program for the representation and manipulation of crystal structures and calculation of the resulting X-ray powder patterns. *J. Appl. Crystallogr.* **1996**, *29*, 301–303. [[CrossRef](#)]
37. Spek, A.L. Single-crystal structure validation with the program PLATON. *J. Appl. Crystallogr.* **2003**, *36*, 7–13. [[CrossRef](#)]
38. Antonio Zárate, J.; Sánchez-González, E.; Jurado-Vázquez, T.; Gutiérrez-Alejandre, A.; González-Zamora, E.; Castillo, I.; Maurin, G.; Ibarra, I.A. Outstanding reversible H₂S capture by an Al(III)-based MOF. *Chem. Commun.* **2019**, *55*, 3049–3052. [[CrossRef](#)]
39. Georgiadis, A.G.; Charisiou, N.; Yentekakis, I.V.; Goula, M.A. Hydrogen Sulfide (H₂S) Removal via MOFs. *Materials* **2020**, *13*, 3640. [[CrossRef](#)]
40. Dong, Q.; Guo, Y.; Cao, H.; Wang, S.; Matsuda, R.; Duan, J. Accelerated C₂H₂/CO₂ Separation by a Se-Functionalized Porous Coordination Polymer with Low Binding Energy. *ACS Appl. Mater. Interfaces* **2020**, *12*, 3764–3772. [[CrossRef](#)]
41. Díaz-Ramírez, M.L.; Vargas, B.; Raziél Álvarez, J.; Landeros-Rivera, B.; Rivera-Almazo, M.; Ramos, C.; Flores, G.; Morales, E.; Vargas, R.; Garza, J.; et al. Fluorometric detection of iodine by MIL-53(Al)-TDC. *Dalton Trans.* **2020**, *49*, 6572–6577. [[CrossRef](#)] [[PubMed](#)]
42. Sim, J.; Yim, H.; Ko, N.; Choi, S.B.; Oh, Y.; Park, H.J.; Park, S.Y.; Kim, J. Gas adsorption properties of highly porous metal–organic frameworks containing functionalized naphthalene dicarboxylate linkers. *Dalton Trans.* **2014**, *43*, 18017–18024. [[CrossRef](#)] [[PubMed](#)]
43. Yao, S.; Wang, D.; Cao, Y.; Li, G.; Huo, Q.; Liu, Y. Two stable 3D porous metal–organic frameworks with high performance for gas adsorption and separation. *J. Mater. Chem. A* **2015**, *3*, 16627–16632. [[CrossRef](#)]
44. Ding, Q.-R.; Wang, F. A pillared-layer framework with high uptake and selective sorption of light hydrocarbons. *Dalton Trans.* **2016**, *45*, 7004–7007. [[CrossRef](#)]
45. Lin, R.B.; Xiang, S.; Zhou, W.; Chen, B. Microporous Metal–Organic Framework Materials for Gas Separation. *Chem* **2020**, *6*, 337–363. [[CrossRef](#)]
46. Sapchenko, S.A.; Barsukova, M.O.; Belosludov, R.V.; Kovalenko, K.A.; Samsonenko, D.G.; Poryvaev, A.S.; Sheveleva, A.M.; Fedin, M.V.; Bogomyakov, A.S.; Dybtsev, D.N.; et al. Understanding Hysteresis in Carbon Dioxide Sorption in Porous Metal–Organic Frameworks. *Inorg. Chem.* **2019**, *58*, 6811–6820. [[CrossRef](#)]
47. Rigaku Oxford Diffraction. *CrysAlisPro 1.171.38.46*; Rigaku Oxford Diffraction: The Woodlands, TX, USA, 2015.
48. Sheldrick, G.M. SHELXT—Integrated space-group and crystal-structure determination. *Acta Crystallogr.* **2015**, *A71*, 3–8. [[CrossRef](#)]
49. Sheldrick, G.M. Crystal structure refinement with SHELXL. *Acta Crystallogr.* **2015**, *C71*, 3–8. [[CrossRef](#)]
50. Pishchur, D.P.; Kompankov, N.B.; Lysova, A.A.; Kozlova, S.G. Order-disorder phase transitions in Zn₂(C₈H₄O₄)₂·C₆H₁₂N₂ in atmospheres of noble gases. *J. Chem. Thermodyn.* **2019**, *130*, 147–153. [[CrossRef](#)]

